Title

Fiber-based platform for synchronous imaging of endogenous and exogenous fluorescence of biological tissue.

Journal

Optics Letters, 44(13)

ISSN

0146-9592

Authors

Alfonso-Garcia, Alba
Li, Cai
Bec, Julien
et al.

Publication Date

2019-07-01

DOI

10.1364/ol.44.003350

Peer reviewed

Published in final edited form as:

Opt Lett. 2019 July 01; 44(13): 3350–3353. doi:10.1364/OL.44.003350.

Fiber-based platform for synchronous imaging of endogenous and exogenous fluorescence of biological tissue

Alba Alfonso-Garcia[1], **Cai Li**[1], **Julien Bec**[1], **Diego Yankelevich**[1,2], **Laura Marcu**[1,*], **Ben Sherlock**[1]

[1]Department of Biomedical Engineering, University of California, Davis, 451 E. Health Sciences Dr., Davis, California 95616, USA

[2]Department of Electrical and Computer Engineering, University of California, Davis, One Shields Avenue, Kemper Hall, Davis, California 95616, USA

Abstract

Endogenous and exogenous fluorescence emission from biological samples encodes complementary information. Here we report, to the best of our knowledge, the first results from an optical imaging platform with interleaved excitation and detection of exogenous and endogenous fluorescence from tissue samples using a single flexible multimode fiber that delivers the excitation beam and collects the emitted light. A custom-built reflective optical chopper wheel with synchronized rotation temporally multiplexes an autofluorescence lifetime imaging apparatus with an intensity-based fluorescence module tailored to imaging green fluorescent protein. We demonstrate the functionality of such platform imaging dyes of varying fluorescence signatures and resolving cellularized areas on bio-engineered tissue constructs.

Laser-induced fluorescence imaging has been a key enabling technology for biological discovery for decades. Sample fluorescence may derive from endogenous or exogenous sources. Endogenous fluorescence originates from naturally occurring fluorescent compounds, including structural proteins (e.g., elastin and collagens), lipids, or cellular metabolic cofactors [e.g., nicotinamide adenine dinucleotide (NADH) and flavin adenine dinucleotide (FAD)] [1-4]. Autofluorescence enables the monitoring of changes in biochemical structure, function, and composition without the potential perturbation or toxicity of external labels. However, endogenous fluorescence has low specificity and weak signals that are frequently signal-to-noise or background limited. Exogenous fluorescence originates from external dyes and molecular probes that label specific cellular or tissue components, and yield strong and bright fluorescence with known spectral signatures [5]. There is considerable interest in developing fluorescence imaging platforms that are capable of *in-situ* examination of live tissues both *in vitro* and *in vivo*. Such platforms can play an important role in research into clinical diagnosis of human diseases such as cancer or atherosclerosis, by enabling the study and monitoring of mechanisms behind disease progression, tissue development, or tissue response to environmental factors. In this Letter, we present a fiber-based approach for interleaved measurements of the endogenous and

*Corresponding author: lmarcu@ucdavis.edu.

exogenous fluorescence from tissue, and demonstrate the functionality of such a platform on bio-engineered tissue constructs.

Scaffold recellularization is a key step for the development of engineered tissues [6] and has been the subject of monitoring through optical imaging. One common strategy to resolve cells on collagenous backgrounds such as bio-engineered blood vessels or other tissue constructs, is by fluorescence imaging of transfected cells expressing green fluorescent protein (GFP) [7-9]. Label-free fluorescence alternatives for monitoring such processes are hindered by a significant spectral overlap between the endogenous fluorescence of structural proteins and cells upon ultraviolet laser light excitation [1,10,11]. Introducing time-resolved measurements of endogenous fluorescence enables further discrimination and has been used to map the distribution of cells on tissue engineered constructs [12]. Furthermore, fluorescence lifetime has the potential to provide additional information on cellular metabolism. A fluorescence lifetime microscopy study by Stringari *et al.* identified stem cells from differentiated epithelial cells in *ex-vivo* small intestine crypts by combining GFP labeled stem cells and NADH autofluorescence, which also unveiled a metabolic gradient in the small intestine villi [13]. Shrestha *et al.* developed a microscope-based technique for interleaved imaging of endogenous and exogenous fluorophores in arteries that employed arrays of dichroic beam splitters to overlap and separate endogenous and exogenous fluorescence [14]. Pedretti *et al.* presented a dualcolor fluorescence lifetime endomicroscope that temporally offsets two lasers that excite endogenous fluorescence from lung tissue and exogenous fluorescence from bacterial infections [15]. While these examples illustrate the complementary nature of endogenous and exogenous fluorescence imaging, opportunities for clinical translation are limited by spectral bandwidth constraints or the use of bulk optical components.

The proposed approach avoids the complexity and spectral bandwidth constraints imposed by additional dichroic beam splitters. The key enabling technology was the development of a custom-built reflective optical chopper wheel (ROCW), the rotation of which allowed the temporal multiplexing of two independent imaging systems: a multispectral fluorescence lifetime imaging (FLIm) system that detects endogenous tissue fluorescence excited at 355 nm, and an intensity-based fluorescence imaging system tailored to detect exogenous fluorescence from enhanced GFP (eGFP). Furthermore, the platform uses a single, flexible, 400 μm core, 0.22 NA multimode fiber (MMF) as an interface between the apparatus and the sample allowing imaging in environments which are inaccessible to microscope-based techniques. For this Letter, the fiber probe was raster scanned across the samples using a 3D translation stage (single pixel acquisition time was 48 ms and the scanning speed in x was 4.17 mm/s; Parker, U.S.) to acquire images of relatively flat samples. Helical scanning mechanisms with side-viewing fiber probes are envisaged for intraluminal imaging of tubular samples. Below, we describe the imaging platform and the technical performance tests conducted on synthetic dyes and tissue constructs.

Endogenous fluorescence was recorded by a mutlispectral FLIm system [16]. As depicted in Fig. 1(a), a 355 nm Q-switched microchip pulsed laser (<0.6 ns pulse width, >0.9 μJ pulse energy, 2 kHz pulse repetition rate, TEEM photonics STV-02E, Meylan, France) was coupled to a MMF probe that delivered pulsed laser light with an average power of 1.8 mW

to the sample. The same MMF collected backscattered tissue autofluorescence and guided it to a wavelength selection module (spectral bands: SB1, 381–399 nm; SB2, 415–440 nm; SB3, 465–553 nm; SB4, 572–642 nm) that used temporal multiplexing to allow multispectral detection using a single photomultiplier tube [16]. Fluorescence decays were acquired using the pulse sampling technique [17,18], and average lifetimes were extracted using a constrained least-squares deconvolution with Laguerre expansion [19].

Exogenous fluorescence was excited by a continuous-wave 450 nm laser diode (PLT5 450B, Osram, Germany), modulated by the ROCW to 250 μs duration pulses at a repetition rate of 2 kHz. At the MMF output, the average power of the 450 nm light was 6.3 mW. Backscattered exogenous fluorescence was collected by the MMF and guided back to the apparatus. A single dichroic beam splitter reflected exogenous fluorescence through a spectral cleanup filter (510/84 nm, FF01-51084, Semrock, Rochester, New York), whereafter it was detected by a photodiode with built in a variable gain trans impedance amplifier (Newport 2001-FS, U.S.). The amplified photodiode output was digitized by the same DAQ board used by the FLIm system. The current exogenous system was designed to detect eGFP fluorescence (emission peak at 509 nm). However, we emphasize here that any optically accessible dye and label can be imaged without requiring any change to the FLIm system. The spatial separation between the exogenous and the FLIm systems afforded by the ROCW ensure they do not interfere.

The fluorescence imaging platform operates by interleaving the excitation and detection of exogenous and endogenous fluorescence [Fig. 1(b)]. Synchronization was provided by a high-speed four-channel digital pulser (Sapphire 9200 Series Pulse Generator, Quantum Composer, Montana, U.S.). One pulser channel triggered the pulsed emission of the 355 nm laser used to excite endogenous fluorescence, while a second channel was used to phase lock the rotation of a custom-built ROCW and to synchronize the acquisition window. The ROCW consisted of a circular disk of 30 periodically reflective (mirror) and transmissive (air gap) sections, mounted on a conventional optical chopper system (MC2000-B, Thorlabs). By controlling the relative phase between the pulser channel used to trigger the laser and the channel controlling the ROCW rotation, we engineered the ROCW to function as a reflective element for the exogenous fluorescence system, and a transmissive element for the FLIm system. The low repetition rate (2 kHz) and duty cycle ($1.2e^{-4}$%) of the FLIm laser ultimately provided the opportunity to adopt this mechanical approach to interleaving the two imaging systems. Representative time-resolved fluorescence signals from the exogenous and endogenous systems, recorded in parallel, are shown in Fig. 1(c). The absence of measurable optical crosstalk between endogenous and exogenous signals provides the first indication that the ROCW is able to effectively isolate the two systems from one another.

To characterize the technical performance of the exogenous imaging system, we compared the fluorescence images acquired from a phantom consisting of five glass capillaries filled with fluorescein dye (similar spectra characteristics as eGFP, emission maximum at 510 nm) dissolved in ethanol at increasing concentrations (0.1, 0.5, 1, 5, and 10 mM) when the ROCW was either held stationary or rotated at a chopping frequency of 2 kHz. Fluorescence intensity images (i), line profiles (ii), and voltage versus concentration curves (iii) obtained

with either mode are shown in Figs. 2(a) and 2(b). The detection threshold (>0.5mM) and the modulation depth of the line profiles were unaffected by transitioning from a stationary to rotating ROCW, which demonstrates that the rotation of the ROCW does not impact the image quality of the exogenous system. Additionally, there was a strong correlation (R^2 = 0.999) between the photodiode voltage recorded in stationary and rotation modes [Fig. 2(c)], and a signal loss of 17% with respect to the stationary mode.

To further assess the ability of the imaging platform to resolve the fluorescence emission (both spectrally and temporally), we imaged six glass capillaries filled with different fluorophore solutions: Coumarin 440 (100 μM in EtOH), Coumarin 460 (100 μM in EtOH), Fluorescein (10 mM in EtOH), and Rhodamine 6G (100 μM in EtOH), and cofactors NADH (250 μM in 0.1 M MOPS buffer) and FAD (2 mg/ml in pure water). Figure 3 shows all the fluorescence images obtained during a single acquisition. From the FLIm system, the fluorescence intensity in each spectral band normalized to the sum of intensities in all spectral bands, a.k.a., intensity ratio images [Fig. 3(a)] and fluorescence lifetime maps [Fig. 3(b)]; from the exogenous system, the normalized fluorescence intensity image [Fig. 3(c)]. The images in Fig. 3(a) demonstrate there is spectral overlap between different fluorophores (i.e., Fluorescein, Rhodamine 6G, and FAD) which may complicate discrimination based solely on the intensity ratio, when excited with UV. This may be overcome by their different lifetime values [Fig. 3(b)]. On the other hand, the image generated by the exogenous system exclusively reports the presence of the Fluorescein filled capillary [Fig. 3(c)]. This simplified example suggests that combined FLIm and exogenous fluorescence can provide enhanced specificity to improve the discrimination of features of interest in biological samples.

The utility of the platform to image biological samples was investigated with a collagenous scaffold that was locally seeded with stem cells, a simplified TEVG recellularization model. The presented imaging platform has the potential to be used for non-destructive, *in situ* monitoring cell-tissue interactions in physiologically relevant geometries (e.g., intraluminal imaging). For instance, the labeling of migration- versus proliferation-specific proteins may elucidate recellularization patterns, while endogenous fluorescence lifetime maps would report on structural changes and metabolic activity distribution along the cellularized area. Here 5 h prior to imaging, antigen-removed bovine pericardium [20] was locally seeded (constrained by glass cylinders, 4 mm inner diameter) with eGFP ubiquitously labeled human mesenchymal stem cells (hMSC), obtained as described in Ref. [21], at densities of 10, 20, 40, and 80 k cells/mm^2. After imaging, the sample was scanned for validation with a conventional fluorescence microscope (using GFP filter configuration with Ex. 470/40 nm, Em. 525/50 nm, dichroic mirror at 495 nm; BZ-X710 fluorescence microscope, Keyence, Itasca, Illinois) using a 4 × /0.13 NA objective lens (Plan Fluor, Nikon). The resulting images are shown in Fig. 4.

Figures 4(a) and 4(b) show the exogenous fluorescence images acquired with the fluorescence microscope and the fiber-based exogenous fluorescence system, respectively. Figures 4(c) and 4(d) show the endogenous intensity ratio and lifetime images acquired in SB3. The seeded areas are marked 1 through 4 in Fig. 4(a) in the order of ascending cell density. An acellular scaffold area (5) and a background location outside the tissue (6) are

also marked for reference. The average intensity and lifetime values from these areas were used to compare the results acquired with either setup. The eGFP fluorescence intensity recorded with the exogenous fluorescence system shows excellent correlation (R^2 = 0.995) with fluorescence microscopy [Fig. 4(e)]. These measurements indicate the utility of the exogenous imaging system to offer similar sensitivities to eGFP fluorescence as a conventional microscope objective, while operating with a flexible MMF interface and in parallel with the endogenous imaging system. Collagen autofluorescence, still strong around 510 nm, is also detected by both exogenous fluorescence imaging apparatus. The endogenous fluorescence at 355 nm excitation is further impacted by the collagen autofluorescence contribution in the spectral band where the autofluorescence from the cells is strongest (SB3, 532–553 nm, tailored for FAD emission). We have previously reported that eGFP excited at 355 nm makes no measurable contribution to the fluorescence detected in this SB3 [12]. In this case, fluorescence lifetime better resolves cells [Fig. 4(d)] than the intensity ratio, which appears homogeneous [Fig. 4(c)]. The antigen-removed bovine pericardium has a long average lifetime of ~5.5 ns, whereas the average lifetimes in the cell seeded areas are depressed by 100–500 ps, depending on the number of cells contributing to the overall signal. The fluorescence lifetime values in SB3 decrease with increasing cell density and negatively correlate (R^2 = 0.997) with the eGFP fluorescence intensity as detected with the fluorescence microscope [Fig. 4(f)].

The need for rapid clinical diagnosis and the advent of engineered tissues have triggered the need for imaging tools that can non-destructively monitor large tissue areas of intricate geometries over time. Fluorescence imaging has demonstrated value to monitor the variety and complexity of biological processes involved with disease and tissue regeneration. Using both endogenous and exogenous fluorescence may be required to provide a more complete picture of biochemical, structural, and functional changes at the sample surface. Furthermore, imaging via flexible fiber optic probes allows *in vivo* interrogation of complex tissue architectures in real time, potentially addressing some of the limitation in three dimensional tissue imaging [22]. Here we present a fiber-based fluorescence imaging platform able to acquire endogenous and exogenous fluorescence images in parallel. Endogenous fluorescence imaging provides a label-free method of visualizing non-specific biochemical changes in the tissues, while exogenous fluorescence imaging provides enhanced specificity for protein-targeted functional analysis. The phase-matched rotation of a ROCW provides the temporal multiplexing of pulses of fluorescence excitation and emission. The ROCW has a broad spectral bandwidth and, thus, provides the flexibility to adapt the platform to image virtually any exogenous dye or label. Furthermore, this approach could be used to multiplex fluorescence imaging with other optical techniques such as spontaneous Raman, Brillouin or non-imaging techniques such as laser ablation.

Acknowledgments

Funding. National Institutes of Health (NIH) (R01HL121068, R03EB025565); California Institute for Regenerative Medicine (CIRM) (RT3-07879).

REFERENCES

1. Croce A and Bottiroli G, Eur. J. Histochem 58, 2461 (2014). [PubMed: 25578980]

2. Marcu L, French PM, and Elson DS, Fluorescence Lifetime Spectroscopy and Imaging: Principles and Applications in Biomedical Diagnostics (CRC Press, 2014).
3. Lakowicz JR, Principles of Fluorescence Spectroscopy, 3rd ed., (Springer Science and Business Media, 2006).
4. Skala MC, Riching KM, Gendron-fitzpatrick A, Eickhoff J, Eliceiri KW, White JG, and Ramanujam N, Proc. Natl. Acad. Sci. USA 104, 19494 (2007). [PubMed: 18042710]
5. Sabnis RW, Handbook of Fluorescent Dyes and Probes (Wiley, 2015).
6. Scarrit ME, Front. Bioeng. Biotechnol 3, 1 (2015). [PubMed: 25654078]
7. Whited BM, Hofmann MC, Lu P, Xu Y, Rylander CG, Wang G, Sapoznik E, Criswell T, Lee SJ, Soker S, and Rylander MN, PLoS ONE 8, e61275 (2013). [PubMed: 23585885]
8. Liu Y, Sakai S, and Taya M, Heliyon 2, e00067 (2016). [PubMed: 27441246]
9. Niu G, Sapoznik E, Lu P, Criswell T, Mohs AM, Wang G, Lee S-J, Xu Y, and Soker S, J. Tissue Eng. Regen. Med 10, 955 (2016). [PubMed: 24616385]
10. Smith LE, Smallwood R, and Macneil S, Microsc. Res. Tech 73, 1123 (2010). [PubMed: 20981758]
11. Georgakoudi I, Jacobson BC, Mu MG, Sheets EE, Badizadegan K, Carr-locke DL, Crum CP, Boone CW, Dasari RR, Dam JV, and Feld MS, Cancer Res. 62, 682 (2002). [PubMed: 11830520]
12. Alfonso-Garcia A, Shklover J, Sherlock BE, Panitch A, Griffiths LG, and Marcu L, J. Biophotonics 11, e201700391 (2018). [PubMed: 29781171]
13. Stringari C, Edwards RA, Pate KT, Waterman ML, Donovan PJ, and Gratton E, Sci. Rep 2, srep00568 (2012).
14. Shrestha S, Serafino MJ, Rico-Jimenez J, Park J, Chen X, Zhaorigetu S, Walton BL, Jo JA, and Applegate BE, Biomed. Opt. Express 7, 3184 (2016). [PubMed: 27699091]
15. Pedretti E, Tanner MG, Choudhary TR, Krstajić N, Megia-Fernandez A, Henderson RK, Bradley M, Thomson RR, Girkin JM, Dhaliwal K, and Dalgarno PA, Biomed. Opt. Express 10, 181 (2018). [PubMed: 30775092]
16. Yankelevich DR, Ma D, Liu J, Sun Y, Sun Y, Bec J, Elson DS, and Marcu L, Rev. Sci. Instrum 85, 034303 (2014). [PubMed: 24689603]
17. Pfefer TJ, Paithankar DY, Poneros JM, Schomacker KT, and Nishioka NS, Lasers Surg. Med 32, 10 (2003). [PubMed: 12516065]
18. Butte PV, Fang Q, Jo JA, Yong WH, Pikul BK, Black KL, and Marcu L, J. Biomed. Opt 15, 027008 (2010). [PubMed: 20459282]
19. Liu J, Sun Y, Qi J, and Marcu L, Phys. Med. Biol 57, 843 (2012). [PubMed: 22290334]
20. Wong ML, Wong JL, Athanasiou KA, and Griffiths LG, Acta Biolmater. 9, 6492 (2013).
21. Liu ZZ, Wong ML, and Griffiths LG, Sci. Rep 6, 1 (2016). [PubMed: 28442746]
22. Antoni D, Burckel H, Josset E, and Noel G, Int. J. Mol. Sci 16, 5517 (2015). [PubMed: 25768338]

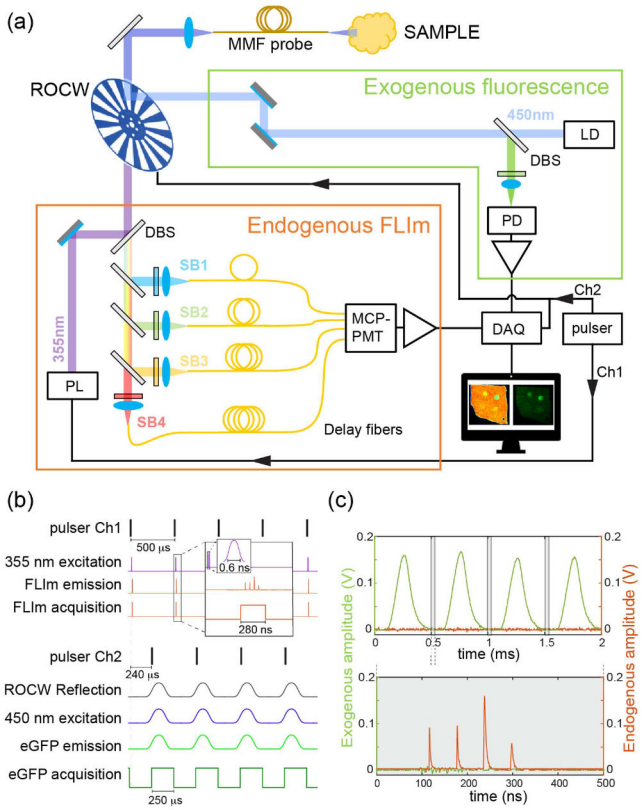

Fig. 1.

(a) Fiber-based imaging apparatus with two independent imaging systems: endogenous FLIm and exogenous intensity-based fluorescence imaging. MMF, multimode fiber; ROCW, reflective optical chopper wheel; DBS, dichroic beam splitter; LD, laser diode; PD, photodiode; PL, pulsed laser; MCP-PMT, microchannel plate-photomultiplier tube; DAQ, data acquisition board. (b) Pulser, excitation, emission, and acquisitions time sequence, and synchronization scheme. (c) Output measurements, exogenous green fluorescence amplitude (left axis); endogenous fluorescence lifetime waveform (right axis).

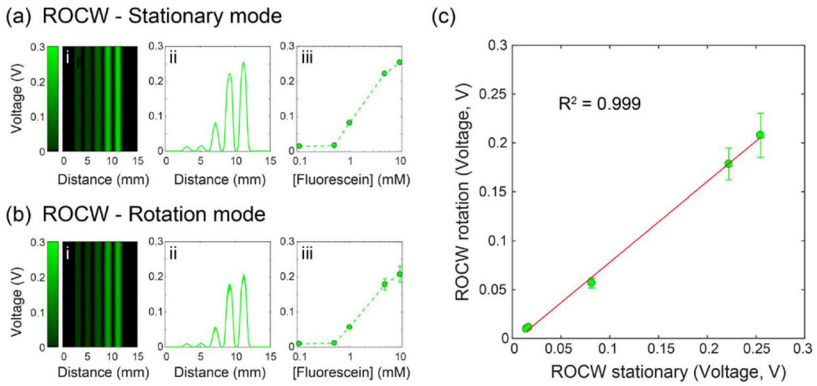

Fig. 2.

Exogenous fluorescence intensity-based image and signal quantification of fluorescein dye at concentrations 0.1, 0.5, 1, 5, and 10 mM, when the ROCW is in the (a) stationary mode and (b) rotation mode (chopping frequency of 2 kHz). Panels (i) fluorescence image, (ii) average intensity profile, and (iii) signal as a function of fluorescein concentration. (c) Linear correlation between the ROCW rotation versus the stationary modes. The error bars are the standard deviation.

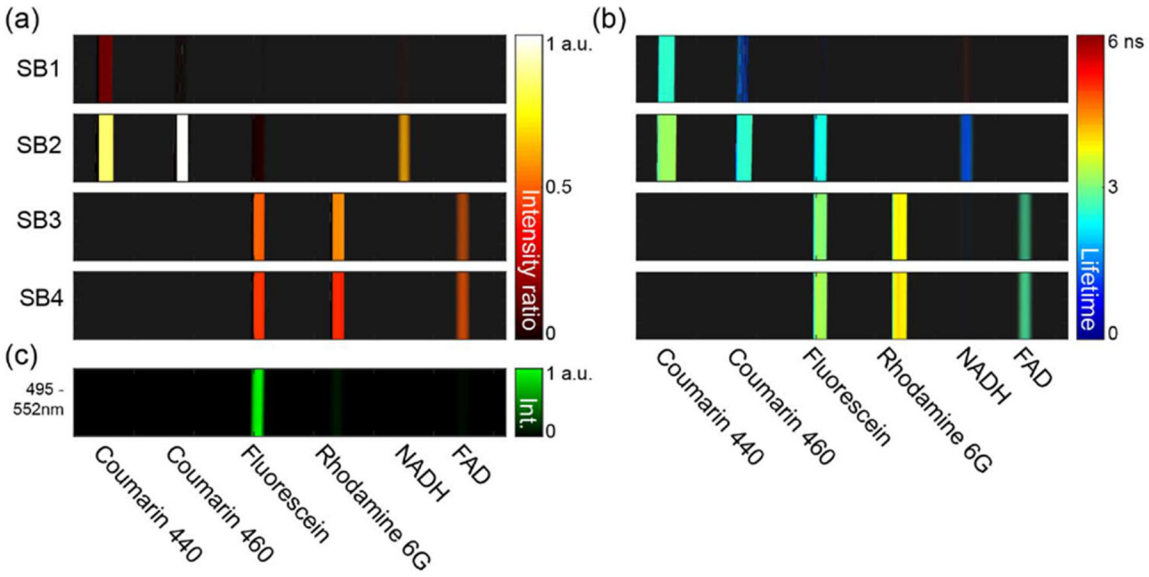

Fig. 3.

Fluorescence intensity and lifetime images from dyes Coumarin 440 (100 μM in EtOH), Coumarin 460 (100 μM in EtOH), Fluorescein (10 mM in EtOH), and Rhodamine 6G (100 μM in EtOH), and organic co-enzymes NADH (250 μM in 0.1M MOPS buffer) and FAD (2 mg/ml in pure H_2O). (a) Intensity ratio and (b) fluorescence lifetime maps obtained with the FLIm system. (c) Normalized fluorescence intensity map obtained with the exogenous imaging system.

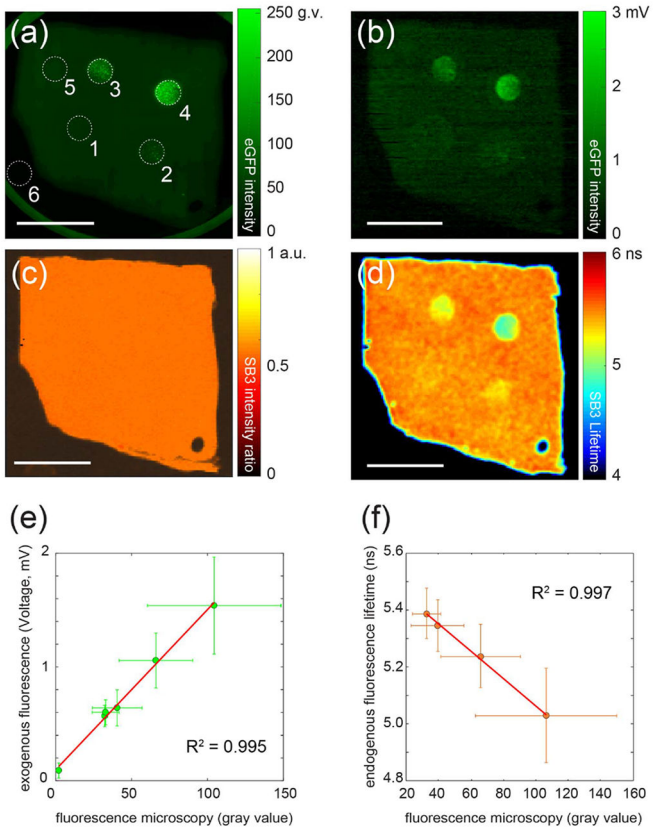

Fig. 4.

Images of antigen-removed bovine pericardium seeded with eGFP-human mesenchymal stem cells at different densities (10, 20, 40, and 80 k cells/mm^2). (a) Fluorescence microscopy image. (b) eGFP image from the exogenous intensity-based fluorescence system. (c) Intensity ratio and (d) fluorescence lifetime maps in SB3 obtained with the endogenous FLIm system. Scale bars: 10 mm. (e) Correlation between the voltage detected with the exogenous system and gray value from the microscope in locations 1 through 6. (f) Correlation between the fluorescence lifetime detected in SB3 and the gray value from the microscope in locations 1 through 4. The error bars are the standard deviation.